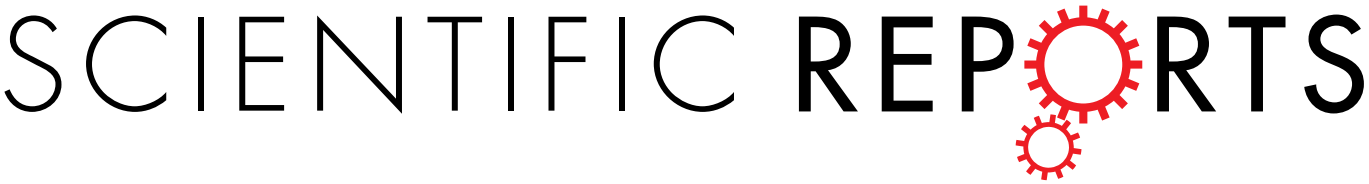

OPEN

Received: 27 April 2016
Accepted: 27 June 2016
Published: 22 July 2016

One-pot hydrothermal synthesis of CuBi co-doped mesoporous zeolite Beta for the removal of NO_x by selective catalytic reduction with ammonia

Zhiguo Xie[1,2], Xiaoxia Zhou[1], Huixia Wu[2], Lisong Chen[1], Han Zhao[1], Yan Liu[1], Linyu Pan[1] & Hangrong Chen[1,3]

A series of CuBi co-doped mesoporous zeolite Beta (Cu_xBi_y-mBeta) were prepared by a facile one-pot hydrothermal treatment approach and were characterized by XRD, N_2 adsorption-desorption, TEM/SEM, XPS, H_2-TPR, NH_3-TPD and *in situ* DRIFTS. The catalysts Cu_xBi_y-mBeta were applied to the removal of NO_x by selective catalytic reduction with ammonia (NH_3-SCR), especially the optimized Cu_1Bi_1-mBeta achieved the high efficiency for the removal of NO_x and N_2 selectivity, superior water and sulfur resistance as well as good durability. The excellent catalytic performance could be attributed to the acid sites of the support and the synergistic effect between copper and bismuth species. Moreover, *in situ* DRIFTS results showed that amides NH_2 and NH_4^+ generated from NH_3 adsorption could be responsible for the high selective catalytic reduction of NO_x to N_2. In addition, a possible catalytic reaction mechanism on Cu_1Bi_1-mBeta for the removal of NO_x by NH_3-SCR was proposed for explaining this catalytic process.

Nowadays, it is still of great challenges for the effectively catalytic purification of diesel exhausts, especially for the NO_x from diesel engine, since the conventional three-way catalysts are no longer effective in selective reducing NO_x[1]. The commercial selective catalytic reduction with ammonia (NH_3-SCR) catalyst for the removal of NO_x, *i.e.*,V_2O_5-WO_3/TiO_2, only shows high catalytic efficiency in a narrow temperature window of 300–400 °C[2], besides, the poor water and sulfur resistance as well as the toxicity of V_2O_5 also greatly prohibit the popularity of vanadium-based composite oxides. Therefore, researchers have devoted to develop a new kind of non-vanadia catalysts to overcome the disadvantages of vanadium-based composite oxides[3]. It was reported that compared to the traditional V_2O_5-WO_3/TiO_2, non-vanadia catalyst not only presents the wider NH_3-SCR temperature windows with high N_2 selectivity, but also owns good durability and strong resistance against H_2O and SO_2.

Very recently, zeolite-based catalysts with high surface areas and pore volume, abundant acidity sites, outstanding thermal and hydrothermal stability, as good catalyst supports, have attracted much research attention in selective catalytic reduction NO_x by ammonia[4,5]. However, small microporous channels of zeolite greatly prevented the diffusion and transport of some large molecules, resulting in the low catalytic performance in a great majority of traditional catalytic reactions[6]. Therefore, a novel zeolite with mesoporous structure has been developed, which combines the advantages of conventional crystalline zeolite and mesoporus material, to enable the quick access for the diffusion and transport attributed to the hierarchically porous structure. It is generally believed that mesoporous zeolites possess remarkably higher catalytic activity and longer catalytic lifetime than

[1]State Key Laboratory of High Performance Ceramics and Superfine Microstructure, Shanghai Institute of Ceramics, Chinese Academy of Sciences, 1295 Dingxi Road, Changning District, Shanghai 200050, P.R. China. [2]The Key Laboratory of Resource Chemistry of Ministry of Education and the Shanghai Key Laboratory of the Rare Earth Functional Materials. Shanghai Normal University, 100 Guilin Road, Xuhui District, Shanghai 200234, P.R. China. [3]National Synergetic Innovation Center for Advanced Materials (SICAM), Jiangsu, China. Correspondence and requests for materials should be addressed to X.Z. (email: xxzhou1983@163.com) or H.C. (email: hrchen@mail.sic.ac.cn)

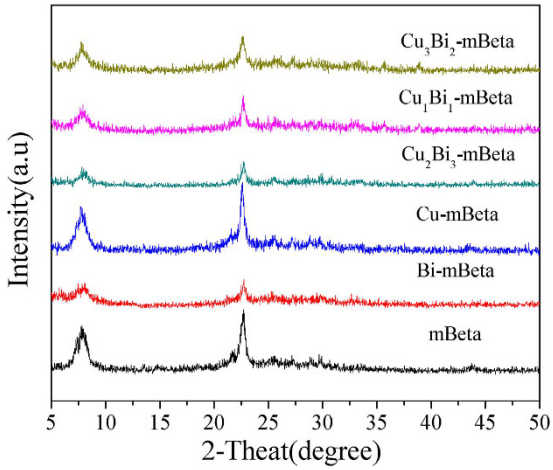

Figure 1. XRD patterns of samples mBeta, Cu-mBeta, Bi-mBeta and Cu_xBi_y-mBeta.

conventional zeolites owing to the crystalline framework and the hierarchically porous structure[7]. Thereinto, the mesoporous Beta zeolite (mBeta) with unique three-dimensional network of large pores (12MR) exhibits much high surface area and excellent hydrothermal stability, which is widely applied in fine chemistry[8]. In the past decades, a number of synthetic approaches of mBeta have been explored and some encouraging results have been obtained[8–10]. Such as, Xiao *et al.*, synthesized highly mesoporous single-crystalline zeolite beta by using a commercial polymer, polydiallyldimethylammonium chloride (PDADMA) as both structure-directing agent and porogen, which showed better hydrothermal stability and higher catalytic activity than conventional zeolite Beta in large molecules involved acid-catalyzed reactions[8]. In addition, many metal oxides were reported to have good performance in the removal of NO_x by NH_3-SCR, *e.g.*, Cu-loaded zeolite beta exhibited a good activity and hydrothermal stability in the NH_3-SCR of NO_x[11,12]. It is also reported that the introduction of Bi_2O_3 can improve the SO_2 resistance[13].

On the basis of our previous work[14], a novel CuBi co-doped mesoporous zeolite Beta (Cu_xBi_y-mBeta) has been synthesized by one-pot hydrothermal treatment approach, by which the copper and bismuth species can be well dispersed into the framework of mesoporous zeolite Beta. Therein, the optimized prepared catalyst Cu_1Bi_1-mBeta exhibits very high catalytic activity for the selective catalytic reduction of NO_x with NH_3. In addition, the N_2 selectivity, water vapor and sulfur resistance and durability of the Cu_1Bi_1-mBeta catalyst have been detailedly investigated. Finally, a possible catalytic mechanism of SCR of NO_x with ammonia on this prepared catalyst CuBi-mBeta is proposed to clarify the catalytic process.

Results

Structure Characteristics. The powder XRD patterns of mBeta, Cu-mBeta, Bi-mBeta and Cu_xBi_y-mBeta are shown in Fig. 1. It is found that all prepared samples keep the diffraction peak of typical zeolite beta structure, and no diffraction peaks corresponding to copper and bismuth species can be detected. Therefore, it is believed that the copper and bismuth species could be well-incorporated into the framework of zeolite as ions or highly dispersed into the mesoporous channels as metal oxides. It is noted that compared with the mBeta, the doping of Bi species can cause the inevitable destruction of zeolite framework to a certain extent, and the intensity of XRD peak of Cu_xBi_y-mBeta decreases with the increase of Bi-loading content, as shown in Fig. 1.

The N_2 adsorption isotherms and pore size distribution curves for samples mBeta, Cu-mBeta, Bi-mBeta and Cu_xBi_y-mBeta are shown in Fig. 2 and the corresponding pore structure parameters of all the samples are summarized in Table 1. All the samples exhibit typical type IV isotherms, confirming the presence of mesoporous structure. The reference sample mBeta shows well-defined mesopore of 3.8 nm, and the BET surface area and total pore volume are calculated to be 556 m^2/g and 0.34 cm^3/g, respectively, including the mesoporous surface area (166 m^2/g) and mesoporous volume (0.16 cm^3/g), respectively. Compared with the mBeta, the surface areas of Cu-mBeta, Bi-mBeta and Cu_xBi_y-mBeta show obvious decrease after loading amount of copper and bismuth species, which is resulted from the generation of non-framework Cu or/and Bi ions (*i.e.*, CuO and Bi_2O_3) with the increase of Cu or Bi content, and inducing the collapse of pore structure of zeolite to some extent. Even so, the prepared Cu_1Bi_1-mBeta still keep high BET surface area and pore volume after doping with Cu and Bi species (Table 1), indicative of the unblocked mesoporous channels due to the high dispersity of Cu and Bi species. It is noted that the optimized Cu_1Bi_1-mBeta with the mesopore size of 3.6 nm shows high BET surface area (539 m^2/g) and total pore volume (0.46 cm^3/g).

The SEM image of as-prepared Cu_1Bi_1-mBeta, as shown in Fig. 3a, presents a rough surface morphology, demonstrating that the mesoporous structure has penetrated into the zeolite crystals by one-pot hydrothermal synthesis process. Additionally, no oxide aggregations can be found, as shown in Fig. 3a,b, indicating that the doped metal oxides are highly dispersed into the carrier mBeta. The clearly crystal lattices can be found in the high-magnification TEM image (Fig. 3c), confirming the zeolite crystallized structure. The element mapping in Fig. 3d–h further confirms that Cu and Bi species are highly dispersed into mesoporous zeolite Beta, which is consistent with the above results of XRD patterns.

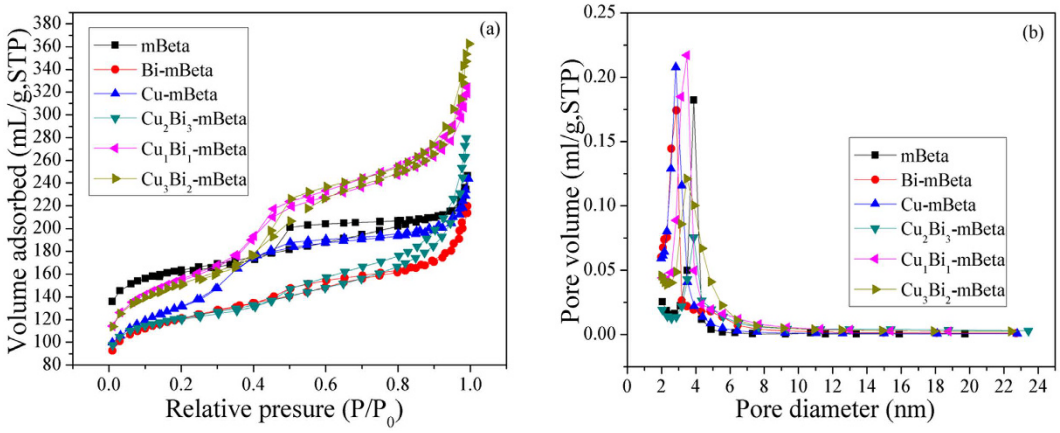

Figure 2. (**a**) N_2 adsorption/desorption isotherms and (**b**) the corresponding pore size distributions of the samples.

Sample	Cu[a] (wt%)	Bi[a] (wt%)	S_{total} (m^2/g)	S_{meso}[b] (m^2/g)	V_{total} (cm^3/g)	V_{meso}[c] (cm^3/g)	Pore diameter (nm)
mBeta	—	—	556	166	0.34	0.16	3.8
Bi-mBeta	—	4.78	413	193	0.31	0.21	2.9
Cu-mBeta	4.4-	—	458	321	0.33	0.27	2.8
Cu_2Bi_3-mBeta	4.32	7.23	415	154	0.36	0.24	3.9
Cu_1Bi_1-mBeta	4.38	4.83	539	304	0.46	0.36	3.6
Cu_3Bi_2-mBeta	6.58	4.77	523	270	0.48	0.35	3.7

Table 1. The composition and structural parameters of the synthesized catalysts. [a]Measured by ICP-AES. [b]S_{meso} was given by the difference between S_{total} and S_{micro}. [c]V_{meso} was given by the difference between V_{total} and V_{micro}.

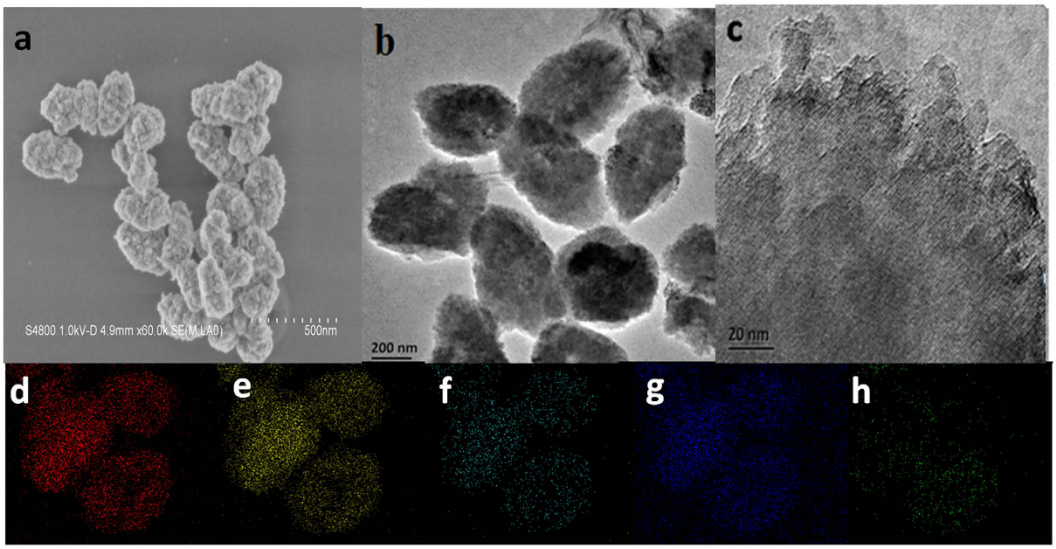

Figure 3. (**a**) Typical SEM images, (**b**) low-magnification TEM images, (**c**) high-magnification TEM images and (**d–h**) the corresponding element mappings of Si, O, Al, Cu and Bi of Cu_1Bi_1-mBeta.

Spectroscopy Characteristics. The X-ray transmission spectroscopy (XPS) result of the Cu_1Bi_1-mBeta is show in Fig. 4a. The binding energy levels of Cu $2p_{3/2}$ and Cu $2p_{1/2}$ at around 934.5 eV and 954.2 eV, respectively (denoted with ★), accompanied by a shoulder peak of about 10 eV higher binding energy, are attributable to Cu(II). Additionally, the distinctive peaks at 936.6 eV and 956.4 eV, (denoted with ▼) can be ascribed

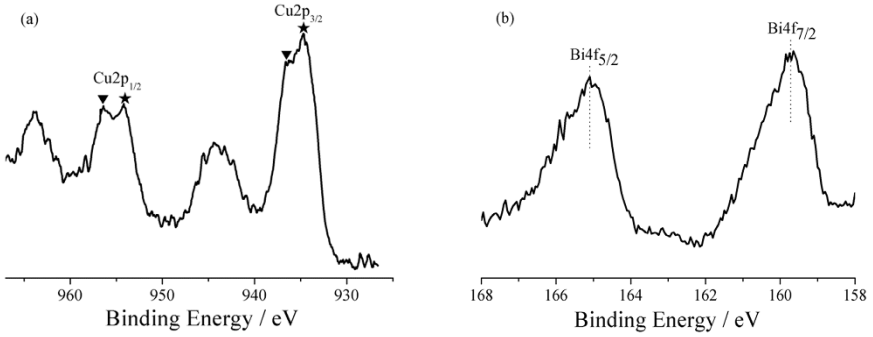

Figure 4. XPS spectra of (**a**) Cu 2p, (**b**) Bi 4f on the Cu_1Bi_1-mBeta catalyst.

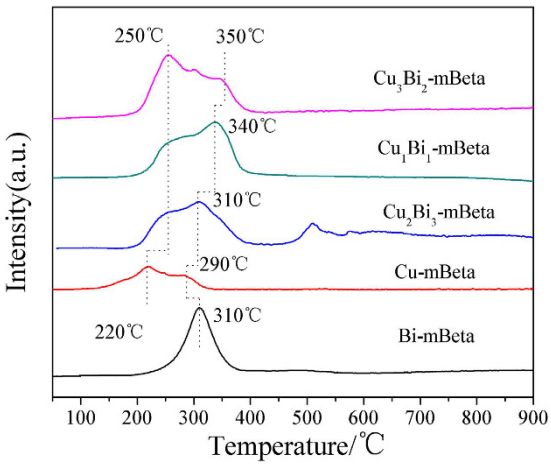

Figure 5. H_2-TPR profiles of Cu-mBeta, Bi-mBeta and Cu_xBi_y-mBeta samples.

to Cu(I), indicating that Cu species have variable valencies in the obtained sample Cu_1Bi_1-mBeta. In addition, the prepared Cu_1Bi_1-mBeta presents higher binding energy peak intensities of Cu(II) (934.5 eV) than that of Cu(I) (936.6 eV), as shown in Fig. 4a, suggesting that Cu_1Bi_1-mBeta contains much more amounts of Cu(II) than Cu(I)[15,16]. Figure 4b shows the Bi 4f XPS spectrum of Cu_1Bi_1-mBeta catalyst. Compared to pure Bi_2O_3 at 164.2 eV and 158.9 eV, the Cu_1Bi_1-mBeta shows the Bi $4f_{5/2}$ and Bi $4f_{7/2}$ a little higher binding energies at 164.6 eV and 159.5 eV, respectively, which is attributed to the interaction between Bi and Cu or the support mBeta[17–19].

The H_2-TPR profiles of Cu-mBeta, Bi-mBeta and a series of Cu_xBi_y-mbeta samples are shown in Fig. 5. It is found that the reference single loaded sample Cu-mBeta shows two weak reduction peaks at around 220 °C and 290 °C, indicating a two-step reduction of Cu^{2+} ions, *i.e.,* firstly to Cu^+ and then to Cu[20,21]. In addition, the reduction peak at 310 °C of reference Bi-mBeta can be ascribed to the reduction of Bi_2O_3. The H_2-TPR profiles of co-loaded samples Cu_xBi_y-mBeta show a distinctively different redox behavior from either Cu-mBeta or Bi-mBeta, and present enhanced reduction peak at 250–350 °C, attributed to the strong interaction between the active species CuO and Bi_2O_3. In addition, the reduction peak gradually shifts toward lower temperature range (from 350 to 310 °C) with the increase of Bi content (Fig. 5 and Table 1), confirming that the addition of Bi_2O_3 is beneficial to promote the catalytic redox reaction[22].

NH_3-TPD experiments were carried out to obtain the acidity information of the prepared catalysts, as shown in Fig. 6. It is clear that a low-temperature peak at 150 °C and a high-temperature peak at 300 °C can be observed for the sample mBeta, which is assigned to weakly weak Lewis acid sites and strong Brønsted acid sites, respectively[23,24]. It is noted that all the samples Cu-mBeta, Bi-mBeta and Cu_xBi_y-mBeta show weaker low-temperature peaks than that of the reference mBeta, owing to the part destruction of zeolite framework structure after introducing Cu and Bi species. However, it is interesting that only the Cu_1Bi_1-mBeta shows a similar desorption peak at high-temperature range (300–400 °C) to the mBeta, indicating that the Cu_1Bi_1-mBeta sample still keeps the strong acidity site of mBeta. The presence of rich acidic sites (Brønsted acid and Lewis acid) produced from the framework Al atoms and copper/bismuth species are helpful to the adsorption and activation of NH_3, and thus producing many ammonia species, including NH_2, coordinated NH_3 and ionic NH_4^+, which can greatly promote the selective catalytic reduction of NO_x, as shown in Fig. 7.

The reaction of adsorbed NH_3 species towards $NO + O_2$ was evaluated by the *in situ* IR spectra at 250 °C and the results are shown in Fig. 7. When the catalyst are exposed to NH_3 for the 60 min and purged with N_2, the peaks related to coordinated NH_3 on Lewis acid sites (3125, 3002, 1611, 1245 and 1115 cm^{-1}) and ionic NH_4^+ bound to Brønsted acid sites (3601 and 1440 cm^{-1}) are clearly observed[15,25–27]. Afterwards, the coordinated NH_3

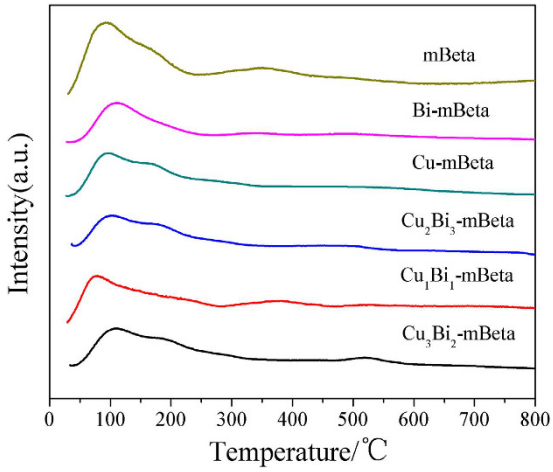

Figure 6. NH_3-TPD profiles of mBeta, Cu-mBeta, Bi-mBeta and Cu_xBi_y-mBeta samples.

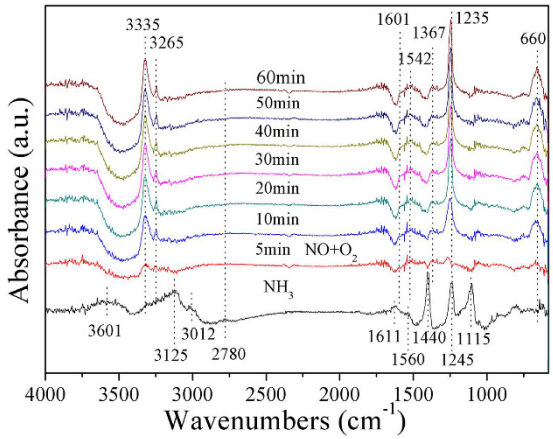

Figure 7. *In situ* DRIFTS spectra over Cu_1Bi_1-mBeta catalyst at 250 °C.

on acidic sites could undergo the oxidative dehydrogenation to form NH_2 species (1560 cm^{-1}), then produce intermediate specie NH_2NO when NO and O_2 were added into reaction gas. It is noted that all the ammonia species, including NH_2, coordinated NH_3 and ionic NH_4^+ bound, disappeared after NO + O_2 purge, indicating that those ammonia species could participate in the reduction of NO_x. Meanwhile, when NO and O_2 were added into reaction gas, the bands at 1235, 1367, 1542 and 1601 cm^{-1} could be detected in IR spectra. Thereinto, the bands at 1235 and 1367 cm^{-1} were assigned to monodentate nitrate, while the bands at 1542 and 1601 cm^{-1} are associated with bidentate nitrate and adsorbed NO_2, respectively[15,25]. More interestingly, two peculiar peaks at 3335 and 3265 cm^{-1} related to the adsorbed NH_3 on acid sites became stronger with the increase of exposing time in the NO + O_2, indicating that some acidic sites on the surface of the catalyst were released and then preferably adsorbed the NH_3 after NO and O_2 pass over the catalyst.

Catalytic performance. Figure 8 shows the NH_3-SCR results of mBeta, Cu-mBeta, Bi-mBeta and a series of Cu_xBi_y-mBeta catalysts. The NO_x conversions over the prepared catalysts under high hourly space velocity of 64000 h^{-1} are shown in Fig. 8a. Compared with the references mBeta, Bi-mBeta and Cu-mBeta, the sample Cu_xBi_y-mBeta show higher catalytic activity for the SCR of NO_x. Especially, the optimized sample Cu_1Bi_1-mBeta with the 4.38 wt% Cu and 4.83 wt% Bi exhibits the highest catalytic performance, *i.e.*, the NO_x conversion efficient is above 90% within the wide operation temperature window of 170 °C to 400 °C. While, the excess doping of Cu and Bi species could induce the formation of oxides aggregates and thus decrease the active surface area (Table 1), *e.g.,* the excess Bi would cover part of active center and results a lower catalytic activity. Therefore, the optimized sample Cu_1Bi_1-mBeta with the 1:1 ratio of Cu and Bi shows the highest catalytic performance. The results of N_2 selectivity of these catalysts were shown in Fig. 8b. For comparison, the reference Bi-mBeta shows a low N_2 selectivity, particular in 200 °C, owing to the part destruction of zeolite framwork with the addition of Bi species, as demonstrated by XRD results, which can affect the strong acidic sites (Fig. 6), thus decrease the adsoption ability of NH_3 on the reference Bi-mBeta. Furthermore, the Cu_1Bi_1-mBeta catalyst also presents as high as up to 100% N_2 selectivity in the whole temperature range investigated. It is believed that the high dispersity of active species

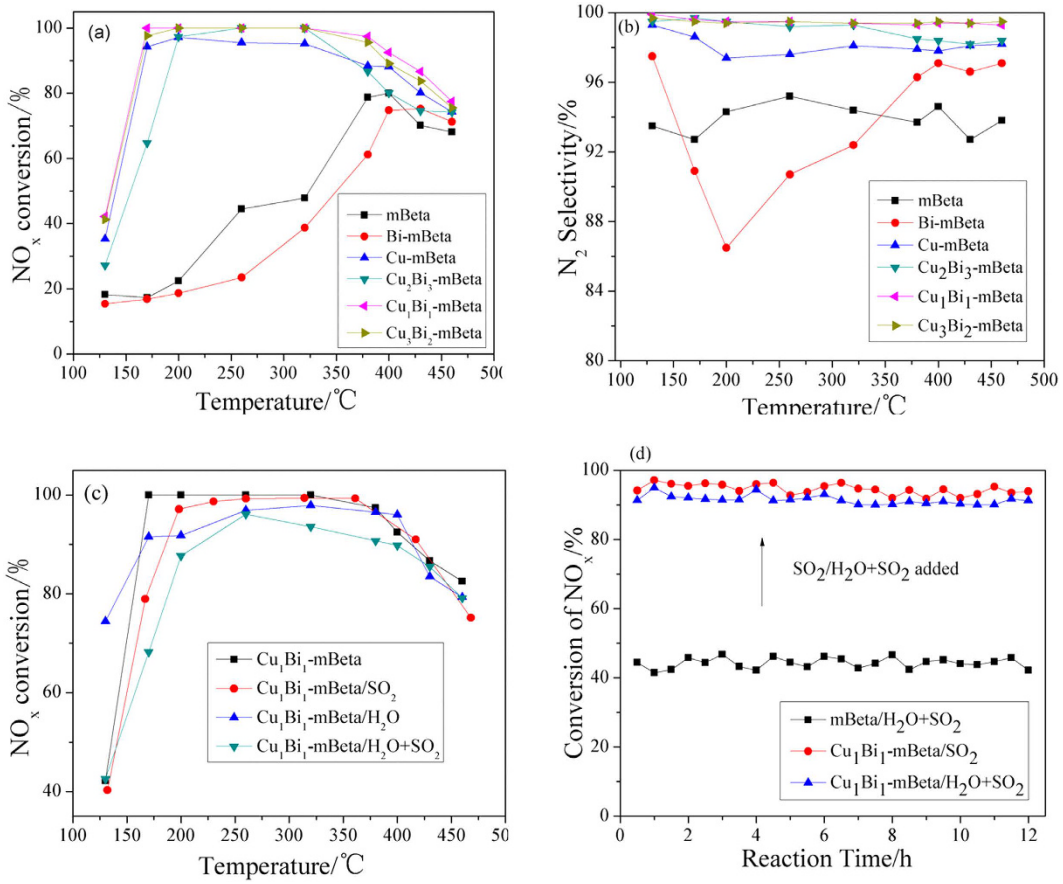

Figure 8. NO_x conversion (**a**), N_2 selectivity (**b**), H_2O and SO_2 resistance (**c**) and durability test at 250°C (**d**) for the NH_3-SCR over mBeta, Cu-mBeta, Bi-mBeta and a series of Cu_xBi_y-mBeta catalysts with different Cu/Bi ratios (500 ppm NO, 500 ppm NH_3, 0 or 3% H_2O, 0 or 50 ppm SO_2, 5% O_2, balance Ar, GHSV = 64 000 h^{-1}).

Cu and Bi on the support mesoporous zeolite, the richer acidic sites and the strong interaction between the active copper and bismuth species on the Cu_1Bi_1-mBeta could be main contributions to the catalytic activity.

It is well known that the real diesel exhaust presents large number of water vapor and trace S compounds, therefore, the effects of H_2O and SO_2 on the SCR catalytic activity are also investigated on the samples Cu_1Bi_1-mBeta. It is evident that compared with the reference mBeta, Cu_1Bi_1-mBeta catalyst shows an excellent SO_2 resistance in the NH_3-SCR above 200 °C (Fig. 8c). Even in the co-presence of H_2O and SO_2, the Cu_1Bi_1-mBeta catalyst still exhibits high activity of over 85% NO_x conversion from 200 °C to 430 °C. The results of durability tested at 250 °C, as shown in Fig. 8d, indicate that the Cu_1Bi_1-mBeta is very stable in the presence of SO_2 (or H_2O and SO_2). It is believed that the highly crystalline zeolite framework enables the catalyst to keep good stability against H_2O, and the highly dispersity active speicies Bi can improve the SO_2 resistance to some extent[13], which is very important for the NH_3-SCR of NO_x in the co-existence of H_2O and SO_2.

Discussion

Based on the above results and discussions, a possible catalytic reaction mechanism for the SCR of NO_x was proposed, as illustrated in Fig. 9. Firstly, there are a large amount of oxygen vacancies (V_0'') presented in the sample support mBeta due to the doping of hetero atoms Cu^{n+}, Bi^{3+} and Al^{3+} in the [SiO_4], leading to the generation of numerous surface activated oxygen (O^*) by adsorbing the O_2, as shown in Step 1 (Fig. 9). Meanwhile, the existence of Bi_2O_3 was reported[22,28] to be beneficial for the reduction of Cu^{2+} to Cu^+, and NO could be easily adsorbed and activated by the Cu^{n+} and generated the $NO^*_{(Cu^{2+})}$ and $NO^*_{(Cu^+)}$ at higher temperatures or lower temperatures, respectively[29,30]. Afterwards, these activated $NO^*_{(Cu^{2+})}$ and $NO^*_{(Cu^+)}$ could react with the surface activated oxygen (O^*) and thus produce large numbers of NO_2, as shown in Step 1 (Fig. 9). When the concentration ratio of NO and NO_2 in reaction gas reaches to 1:1, the quick SCR reaction ($NO + NO_2 + 2NH_3 = 2N_2 + 3H_2O$) occurs, during which the NO_x conversion efficiency at low temperature can be greatly improved. Secondly, the presence of rich acidic sites (Brønsted acid and Lewis acid) produced from the framework Al atoms and copper/bismuth species is helpful to the adsorption and activation of NH_3, *i.e.*, the NH_3 adsorbed on strong Brønsted acid sites could be activated and generate NH_4^+, which was discovered from the *in situ* DRIFTs (Fig. 7), as shown in Step 2 (Fig. 9). Meanwhile, the NH_3 molecules could also be adsorbed on the weak Lewis acid sites to generate $NH_{3(ads)}$ and react with the activated oxygen (O^*) to produce the amines NH/NH_2, as confirmed by the *in situ* DRIFTs (Fig. 7). Finally, the produced amide NH/NH_2 and NH_4^+ could directly react with NO_x on the highly dispersed

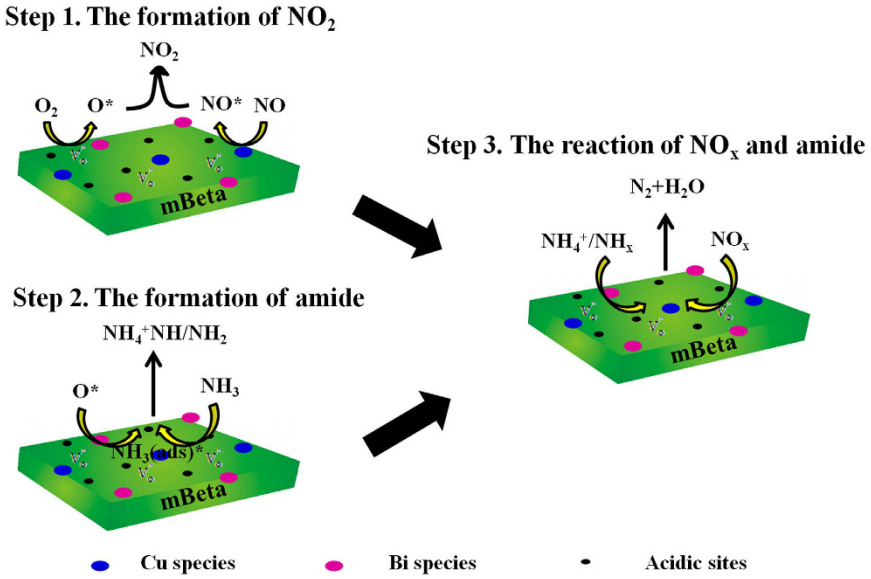

Figure 9. A possible reaction mechanism of NH_3-SCR of NO on Cu_1Bi_1-mBeta catalyst.

active sites and generate N_2, as shown in Step 3 (Fig. 9). It is believed that the existence of highly dispersed varied valence Cu species and acidic sites can accelerate the adsorption and activation of NO and NH_3 in this reaction system, which greatly increases the NH_3-SCR in the removal of NO_x.

In conclusion, a series of Cu_xBi_y-mBeta catalysts have been prepared by a facile one-pot hydrothermal treatment approach. The optimized Cu_1Bi_1-mBeta shows an excellent NH_3-SCR activity and high N_2 selectivity (closely to 100%) toward NO_x in a broad operation temperature window (170–400 °C). On the one hand, the mesopores structure is helpful for the homogeneous dispersion of active species, which can improve the diffusion and transport of reactants and products. Also, the highly crystalline zeolite framework enables the catalyst to keep good resistence toward water vapor. On the other hand, the highly dispersity of copper and bismuth active species, as well as the synergetic catalytic effect between copper and bismuth species and the richer acidic sites of the zeolite promote the reduction of CuO and generation of intermediate NO_2. Meanwhile, the large number of amide NH/NH_2 and NH_4^+ generated from NH_3 adsorption, as the key intermediates, greatly accelerate the selective catalytic reduction of NO_x. More interesting, the prepared catalyst shows good durability and high resistance against H_2O and SO_2, which could also be ascribed to the crystalline zeolite framework and the highly dispersity active sites. The CuBi-mBeta catalyst with distinctive mirco-mesoporous structure demonstrates excellent NH_3-SCR activity and high stability, which, as we believe, will present promising prospect in the practical application of catalytic purification of diesel exhausts.

Methods

Preparation of the mesoporous zeolite Beta (mBeta). Typically, 0.05 g NaCl and 0.15 g KCl were added into 2 mL distilled water and 14.4 g TEAOH solution. Afterwards, 3.9 g H_2SiO_3 was dissolved into the above mentioned solution and stirred at 313 K for 6 h. Next, the solution containing 0.033 g NaOH, 0.17 g $NaAlO_2$ and 2 mL distilled water was slowly added into the resultant solution and further stirred at 313 K for 6 h. Finally, 0.5 g CTAB solution was added into the obtained solution and further stirred at 353 K for 8 h. The obtained mixed solution was hydrothermally treated for 48 h at 423 K. Subsequently, the products were washed with distilled water and dried at 383 K for 12 h. The final product mBeta was obtained after calcinations at 823 K for 6 h to remove any organics.

Preparation of Cu_1Bi_1-mBeta. Typically, 0.05 g NaCl and 0.15 g KCl were added into 2 mL distilled water and 14.4 g TEAOH solution. Afterwards, 3.9 g H_2SiO_3 was dissolved into the above mentioned solution and stirred at 313 K for 6 h. Then, the solution containing 0.033 g NaOH, 0.17 g $NaAlO_2$ and 2 mL distilled water was slowly added into the resultant solution and stirring. Next, 1 mmol $Cu(NO_3)_2{\bullet}3H_2O$, 1 mmol $Bi(NO_3)_3{\bullet}5H_2O$ and 2 mL distilled water was slowly added into the above precursor solution and further stirred at 313 K for 6 h. Then, 0.5 g CTAB solution was added into the obtained solution and further stirred at 353 K for 8 h. Next, the obtained mixed solution was hydrothermally treated for 48 h at 423 K. Subsequently, the products were washed with distilled water and dried at 383 K for 12 h. The final product, Cu_1Bi_1-mBeta, was obtained after calcinations at 823 K for 6 h to remove any organics.

For comparison, the Cu-mBeta, Bi-mBeta and Cu_xBi_y-mBeta were synthesized by a facile one-pot hydrothermal treatment approach, similarly to the above process of Cu_1Bi_1-mBeta. Herein, the x and y represent the millimole amount of Cu and Bi in the initial precursor solution, respectively. In addition, the final pH value of the synthetic gel including copper and bismuth species is about 11.

Sample characterization. The XRD patterns were recorded on a Rigaku D/Max-2200PC X-ray diffractometer using Cu target at 40 kV and 40 mA. The N_2 adsorption and desorption measurements were performed using Micromeritics Tristar 3000 at 77 K. The total surface area and pore volume were calculated using the BET and BJH method. Field emission scanning electron microscopy (SEM) analysis was performed on a JEOL JSM6700F electron microscope. Field emission transmission electron microscopy (TEM) analysis was conducted with a JEOL 200CX electron microscope operated at 200 keV. X-ray photoelectron spectroscopy (XPS) signals were collected on a Thermo Scientific ESCALAB 250 instrument using monochromated Al X-ray resource at 1486.6 eV operated at 15 kW. The temperature-programed reduction with hydrogen (H_2-TPR) and temperature programmed desorption of ammonia (NH_3-TPD) were performed on Micromeritics Chemisorb 2750 instrument attached with ChemiSoft TPx software. TPR was carried out from room temperature to 900 °C under 5% H_2 in Ar at a flow rate of 25 mL/min. The H_2 signal was detected by a thermal conductivity detector (TCD). The NH_3-TPD of the samples was carried out from room temperature to 800 °C at a flow rate of 25 mL/min. The amount of NH_3 desorbed was measured using a thermal conductivity detector (TCD). *In situ* diffuse reflectance infrared Fourier transform spectroscopy (DRIFTS) was performd on a Bruker spectrometer equipped with an MCT detector. Prior to each experiment, the sample was pretreated at 400 °C for 1 h in a flow of N_2 and then cooled down to 200 °C. The background spectrum was collected in flowing N_2 and automatically subtracted from the sample spectrum. The reaction conditions were controlled as follows: 100 mL min^{-1} total flow rate, 500 ppm NH_3, 500 ppm NO, 5% O_2 and N_2 as the balance. All spectra were recorded by accumulating 100 scans with a resolution of 4 cm^{-1}. The contents of Cu and Bi were measured by using Inductively Coupled Plasma Atomic Emission Spectroscopy (ICP-AES) analyzer on a Vista AX.

Catalytic activity test. The catalysis measurements were carried out in a fixed-bed quartz reactor using 0.2 g catalyst of 40–60 meshes. Before catalytic test, the catalysts were dried at 423 K for 16 h. The feed gas mixture contained 500 ppm NO, 500 ppm NH_3, 0 or 3% H_2O, 0 or 50 ppm SO_2, 5% O_2 and Ar as the balance gas. The total flow rate of the feed gas was 300 mL/min, corresponding to a GHSV of 64,000 h^{-1}. The composition of the product gas was analyzed by a chemiluminescence NO/NO_2 analyzer (Thermal Scientific, model 42i-HL) and gas chromatograph (Shimadzu GC 2014 equipped with Porapak Q and Molecular sieve 5A columns). The activity data were collected when the catalytic reaction practically reached steady-state condition at each temperature.

The NO_x (X_{NOx}) and NH_3 (X_{NH3}) conversions and N_2 selectivity (S_{N2}) were calculated as

$$X_{\mathrm{NOx}} = \frac{C^{\mathrm{in}}_{\mathrm{NOx}} - C^{\mathrm{out}}_{\mathrm{NOx}}}{C^{\mathrm{in}}_{\mathrm{NOx}}} \times 100$$

$$X_{\mathrm{NH3}} = \frac{C^{\mathrm{in}}_{\mathrm{NH3}} - C^{\mathrm{out}}_{\mathrm{NH3}}}{C^{\mathrm{in}}_{\mathrm{NH3}}} \times 100$$

$$S_{\mathrm{N2}} = \frac{2C^{\mathrm{out}}_{\mathrm{N2}}}{C^{\mathrm{in}}_{\mathrm{NH3}}X_{\mathrm{NH3}} + C^{\mathrm{in}}_{\mathrm{NOX}}X_{\mathrm{NOX}}} \times 100$$

where NO_x includes NO and NO_2, C_i presents the concentration of the "i" species, and the "in" and "out" present the gas concentration of inlet and the exit of the reactor, respectively.

References

1. Su, W. K., Chang, H. Z., Peng, Y., Zhang, C. Z. & Li, J. H. Reaction pathway investigation on the selective catalytic reduction of NO with NH_3 over Cu/SSZ-13 at low temperatures. *Environ. Sic. Technol.* **49,** 467–473 (2015).
2. Zhang, Q. L. *et al.* Low-temperature selective catalytic reduction of NO with NH_3 over monolith catalyst of MnO_x/CeO_2-ZrO_2-Al_2O_3. *Catal. Today* **175,** 171–176 (2011).
3. Peng, Y., Qu, R. Y., Zhang, X. Y. & Li, J. H. The Relationship between Structure and Activity of MoO_3-CeO_2 Catalysts for NO Removal: Influences of Acidity and Reducibility. *Chem. Commun*. **49,** 6215–6217 (2013).
4. Jin, R. B. *et al.* The role of cerium in the improved SO_2 tolerance for NO reduction with NH_3 over Mn-Ce/TiO_2 catalyst at low temperature. *Appl. Catal. B* **148–149,** 582–588 (2014).
5. Chang, X. F., Lu, G. Z., Guo, Y., Wang, Y. Q. & Guo, Y. L. A high effective adsorbent of NO_x: Preparation, characterization and performance of Ca-beta zeolites. *Microporous Mesoporous Mater*. **165,** 113–120 (2013).
6. Lethbridge, Z. A. D., Williams, J. J., Walton, R. I., Evans, K. E. & Smith, C. W. Methods for the synthesis of large crystals of silicate zeolites. *Microporous Mesoporous Mater*. **79,** 339–352 (2005).
7. Xu, L. *et al.* Enhancement of low-temperature activity over Cu-exchanged zeolite beta from organotemplate-free synthesis for the selective catalytic reduction of NO_x with NH_3 in exhaust gas streams. *Microporous Mesoporous Mater*. **200,** 304–310 (2014).
8. Zhu, J. *et al.* Highly Mesoporous Single-Crystalline Zeolite Beta Synthesized Using a Nonsurfactant Cationic Polymer as a Dual-Function Template. *J. Am. Chem. Soc*. **136,** 2503–2510 (2014).
9. Chen, C. Y. *et al.* Enhanced performance in catalytic combustion of toluene over mesoporous Beta zeolite-supported platinum catalyst. *Appl. Catal. B* **140–141,** 199–205 (2013).
10. Yin, C. Y. *et al.* One-step synthesis of hierarchical mesoporous zeolite Beta microspheres from assembly of nanocrystals. *J. Colloid. Interface Sci*. **397,** 108–113 (2013).
11. Baerdemaeker, T. D. *et al.* Catalytic applications of OSDA-free Beta zeolite. *J. Catal*. **308,** 73–81 (2013).
12. Deka, U., Lezcano-Gonzalez, I., Weckhuysen, B. M. & Beale, A. M. Local Environment and Nature of Cu Active Sites in Zeolite-Based Catalysts for the Selective Catalytic Reduction of NO_x. *ACS Catal*. **3,** 413–427 (2013).
13. Karlsson, H. T. & Rosenberg, H. S. Flue gas denitrification. Selective catalytic oxidation of NO to NO_2. *Ind. Eng. Chem. Proc. Des. Dev*. **23,** 808–814 (1984).
14. Zhou, X. X. *et al.* A facile one-pot synthesis of hierarchically porous Cu(I)-ZSM-5 for radicals-involved oxidation of cyclohexane. *Appl. Catal. A* **451,** 112–119 (2013).

15. Zhang, R. R., Li, Y. H. & Zhen, T. L. Ammonia selective catalytic reduction of NO over Fe/Cu-SSZ-13. *RSC Adv.* **4,** 52130–52139 (2014).
16. Chadwick, D. & Hashemi, T. Adsorbed corrosion inhibitors studied by electron spectroscopy: Benzotriazole on copper and copper alloys. *Corros. Sci* **18,** 39–51 (1978).
17. Bian, Z. F. *et al.* Self-Assembly of Active Bi_2O_3/TiO_2 Visible Photocatalyst with Ordered Mesoporous Structure and Highly Crystallized Anatase. *J. Phys. Chem. C* **112,** 6258–6262 (2008).
18. Shan, W. J., Hu, Y., Zheng, M. M. & Wei, C. H. The enhanced photocatalytic activity and self-cleaning properties of mesoporous SiO_2 coated Cu-Bi_2O_3 thin films. *Dalton Trans.* **44,** 7428–7436 (2015).
19. Jiang, H.-Y. *et al.* Efficient organic degradation under visible light by α-Bi_2O_3 with a CuO_x-assistant electron transfer process. *Appl. Catal. B* **163,** 267–276 (2015).
20. Richter, M. *et al.* Gas-phase carbonylation of methanol to dimethyl carbonate on chloride-free Cu-precipitated zeolite Y at normal pressure. *J. Catal.* **245,** 11–24 (2007).
21. Xue, J. J. *et al.* Characterization of copper species over Cu/SAPO-34 in selective catalytic reduction of NO_x with ammonia: Relationships between active Cu sites and de-NO_x performance at low temperature. *J. Catal.* **297,** 56–64 (2013).
22. Yang, G. H. *et al.* MCM-41 supported CuO/Bi_2O_3 nanoparticles as potential catalyst for 1,4-butynediol synthesis. *Ceram. Int.* **40,** 3969–3973 (2014).
23. Zhou, X. X. *et al.* Dual-mesoporous ZSM-5 zeolite with highly b-axis-oriented large mesopore channels for the production of benzoin ethyl ether. *Chem.-Eur. J.* **19,** 10017–10023 (2013).
24. Wang, D. *et al.* A comparison of hydrothermal aging effects on NH_3-SCR of NO_x over Cu-SSZ-13 and Cu-SAPO-34 catalysts. *Appl. Catal. B* **165,** 438–445 (2015).
25. Liu, Z. M. *et al.* A superior catalyst with dual redox cycles for the selective reduction of NO_x by ammonia. *Chem. Commun.* **49,** 7726–7728 (2013).
26. Meng, D. M. *et al.* A Highly Effective Catalyst of Sm-MnO_x for the NH_3-SCR of NO_x at Low Temperature: Promotional Role of Sm and Its Catalytic Performance. *ACS Catal.* **5,** 5973–5983 (2015).
27. Yu, T. *et al.* Recent NH_3-SCR Mechanism Research over Cu/SAPO-34 Catalyst. *J. Phys. Chem. C* **118,** 6565–6575 (2014).
28. Lin, G. *et al.* Universal Preparation of Novel Metal and Semiconductor Nanoparticle-Glass Composites with Excellent Nonlinear Optical Properties. *J. Phys. Chem. C* **115,** 24598–24604 (2011).
29. Chen, B. H., Xu, R. N., Zhang, R. D. & Liu, N. Economical Way to Synthesize SSZ-13 with Abundant Ion-Exchanged Cu^+ for an Extraordinary Performance in Selective Catalytic Reduction (SCR) of NO_x by Ammonia. *Environ. Sci. Technol.* **48,** 13909–13916 (2014).
30. Zhang, R. Q. *et al.* NO Chemisorption on Cu/SSZ-13: A Comparative Study from Infrared Spectroscopy and DFT Calculations. *ACS Catal.* **4,** 4093–4105 (2014).

Acknowledgements

This research was sponsored by National Key Basic Research Program of China (2013CB933202), China National Funds for Distinguished Young Scientists (51225202) and National Natural Science Foundation of China (51502330).

Author Contributions

Z.X. conceived the preparation method, synthesized and characterization of the CuBi co-doped mesoporous zeolite Beta. Z.X., X.Z., H.W. and H.C. analyzed the experimental results and preparation of the manuscript draft. L.C., H.Z., Y.L. and L.P. supervised and finalized the project. All authors discussed the results and contributed to the final manuscript.

Additional Information

Competing financial interests: The authors declare no competing financial interests.

How to cite this article: Xie, Z. *et al.* One-pot hydrothermal synthesis of CuBi co-doped mesoporous zeolite Beta for the removal of NO_x by selective catalytic reduction with ammonia. *Sci. Rep.* **6**, 30132; doi: 10.1038/srep30132 (2016).